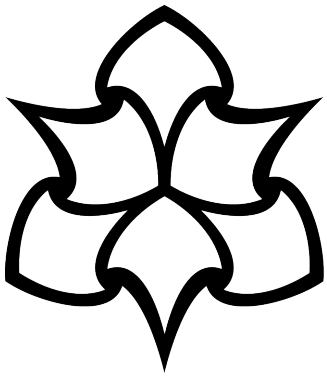

CHEMISTRY OF MATERIALS

Article

pubs.acs.org/cm

General Synthesis Method for Bimetallic Carbides of Group VIIIA First Row Transition Metals with Molybdenum and Tungsten

Yagya N. Regmi and Brian M. Leonard*

Department of Chemistry, University of Wyoming, Laramie, Wyoming 82071, United States

Supporting Information

ABSTRACT: We have established a general method for the synthesis of two different stoichiometries of bimetallic carbides for each of the first row transition metals (TM) of Group VIIIA with tungsten and molybdenum. A dispersion of bimetallic carbide particles in a network of carbon was achieved using excess carbon during the carbothermic reduction process. An investigation into the reduction process revealed bimetallic carbide formation proceeding via stepwise reduction of oxide precursors to metals. The low carbon content phase $TM_6(Mo/W)_6C$ and the high carbon content phase $TM_3(Mo/W)_3C$ form within a temperature window of 60 °C which emphasizes the need for careful control over reaction conditions in order to form the desired phase pure product.

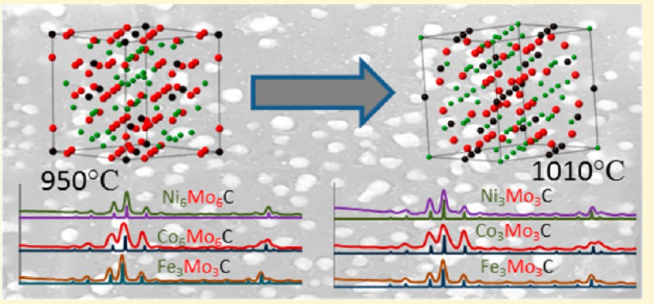

INTRODUCTION

Interest in transition metal (TM) carbides as alternative catalytic materials for several chemical processes such as oxygen reduction reaction (ORR), which typically involve rare and expensive metals like platinum, has inspired numerous investigations into their synthesis and development as catalysts.[1] Tungsten carbide (WC) has been shown to catalyze the formation of water at room temperature, which had not been observed for any other TM besides platinum until the tungsten carbide results were reported in 1973.[2] Since 1973, catalytic activities were also observed, albeit in different reactions, for various other metal carbides such as molybdenum carbide (Mo_2C),[3] iron carbide (Fe_3C),[4,5] and cobalt carbide (Co_2C).[6] Efforts continue to be invested toward optimizing the catalytic activities of monometallic carbides by fine-tuning the electronic properties, morphology, and increasing the specific surface area of various forms of these carbides.[7]

While TM carbides, such as molybdenum carbide, show catalytic activities in reactions involving hydrogen transfer,[8,9] monometallic carbides tend to be unstable under catalytic condition such as in proton exchange membrane (PEM) fuel cells where the catalysts have to withstand highly reducing environment and fluctuating voltage.[10] WC specifically has been proven to be unstable in such environments.[11] Efforts to improve the stability include varying the stoichiometry of these metal carbides, synthesizing polymorphs, and/or supporting them on high surface area materials like carbon nanotubes and silica.[12,13] It has also been observed that the presence of a second TM as either cemented material[14] or as metal nanoparticles supported on the carbide improve the stability and activity of monometallic carbides like WC and Mo_2C.[15]

Increasing the surface area of the catalyst is the most popular route toward optimization of the catalytic activity. However, it has been shown that the mere presence of other TMs such as iron and nickel into either tungsten or molybdenum carbide lattice can also dramatically improve the catalytic activity of these materials.[16,17] The addition of a second TM into the carbide lattice to form bimetallic carbides enables further tuning of the electronic properties of the resulting material.[18] Additionally, cobalt molybdenum carbide was shown to be an excellent alternative to carbon as a support material in ORR.[19] Thus, the synthesis of bimetallic carbides with various crystal structures and stoichiometries is desirable to enhance the investigation of metal carbides as advanced catalysts and/or support materials.

Various methods have been utilized to synthesize bimetallic carbides of the Group VIIIA metals—nickel, cobalt, and iron with tungsten or molybdenum. Earliest attempts employed arc melting that is energy expensive, due to the high temperatures required, and long annealing time employed.[20] One of the major drawbacks of the arc-melting bimetallic carbide products is that they tend to have low specific surface area because of the high temperatures employed. Temperature programmed reduction carburization (TPRC) is another common method that allows reduction of precursor materials at lower temperatures under a flow of hydrocarbon gases that serve as a source of carbon.[21] Although particle size of the TPRC product can be reduced tremendously compared to the arc-melting method, reproducibility and phase purity still have proven to be a challenge.[22] In most cases, the bimetallic carbide products either contain monometallic carbides and elemental metals as impurity or the second metal particles supported on the

Received: January 9, 2014
Revised: March 14, 2014

   dx.doi.org/10.1021/cm500076v | Chem. Mater. XXXX, XXX, XXX–XXX

monometallic carbide crystals instead of being incorporated in the crystal lattice itself. The latter case leads to the formation of cemented carbides instead of bimetallic carbides.[23]

Bimetallic carbides have also been prepared via various intermediates that aid in size control and phase purity. Some of the more successful routes have involved conversion of bimetallic nitrides and oxides via calcination and intermetallic alloys.[24] These methods tend to work for one particular bimetallic carbide system to some extent, but not for others. Specific synthesis methods involving highly specialized resins as a source of carbon have also been reported for particular bimetallic carbides of high purity and good activity.[25] No common synthesis method that is energy efficient and simple has been reported that can be employed to synthesize a broad range of bimetallic carbides of TMs with molybdenum and tungsten until now.

In this work, it is shown that a general method can be employed for all three first row TMs in group VIIIA toward formation of single phase bimetallic carbides of molybdenum and tungsten. Additionally, we employ the same method to prepare two different crystal structures for each system, with high carbon content, $TM_3(Mo/W)_3C$, and low carbon content, $TM_6(Mo/W)_6C$, by varying the annealing temperature the samples are exposed to, i.e., the carbothermic reduction temperature by 60 °C. This method utilizes stable oxide precursors and relatively low carburization temperatures to yield carbides with nanometer dimensions. Dispersion of bimetallic carbide particles is also desirable to prevent agglomeration of high surface area catalyst particles.[26] By simply adding an excess of carbon, islands of bimetallic carbides can be formed on a carbon support. Dispersed bimetallic carbide particles were observed under scanning electron microscope (SEM) for most systems, but reproducibility of the phase pure bimetallic carbide was less consistent. To overcome this phase separation, bimetallic oxides were synthesized using a hydrothermal method and carburized yielding bimetallic carbides with high specific surface area.[27,28] To probe the reduction of the precursor oxides and formation of bimetallic carbides, the reactions were followed using a thermogravimetric analysis instrument equipped with differential scanning calorimetry (TGA/DSC). The results showed stepwise reduction of oxide precursors leading up to metals and then the formation of bimetallic carbides. An investigation into the transitions from low carbon content to high carbon content phases revealed the complete decomposition of the carbide phase and formation of intermetallic alloys of various stoichiometries within the 60 °C temperature window.

■ EXPERIMENTAL SECTION

Materials. NiO (99.8% <50 nm), Co_3O_4 (99.5% <50 nm), and magnetite Fe_3O_4 (95% <5 μm) were used as received from Aldrich. $FeCl_2{\cdot}H_2O$ and $NiCl_2{\cdot}6H_2O$ were purchased from Mallinckrodt. $CoCl_2{\cdot}6H_2O$ and decolorizing carbon were purchased from J. T. Baker. $Na_2MoO_4{\cdot}2H_2O$ was purchased from Sigma, $Na_2WO_4{\cdot}2H_2O$ from Fisher Scientific, MoO_3 from Matheson Coleman & Bell as $H_2MoO_4.H_2O$ containing 99% as MoO_3, and $(NH_4)_6H_2W_{12}O_{40}{\cdot}xH_2O$ (99%) from Fluka. All the reagents were used as purchased except for $(NH_4)_6H_2W_{12}O_{40}{\cdot}xH_2O$ (99%) which was placed inside a Thermo Scientific Thermolyne Furnace (Benchtop Industrial/Type FD1500D) in an alumina boat and heated to 650 °C for 5 h to obtain WO_3 powder.

Carbothermic Reduction of Monometallic Oxides. The metal oxide powders represented by Fe_3O_4 (2.32×10^{-3}moles) and MoO_3 (6.95×10^{-3} mol) were combined with decolorizing carbon to produce 1 to 1 molar ratio of the two metals and either stoichiometric amount or 1 to 18 molar ratio of metal to carbon. The mixture was ground with a mortar and pestle for 20 min to obtain a homogeneous solid mixture. The resulting mixture was transferred to an alumina crucible boat and heated in a furnace to the desired annealing temperatures (AT). The annealing temperatures are detailed in Table S1 (Supporting Information). The furnace was ramped to the annealing temperatures at 1 °C/min under a flow of argon gas. Once the highest temperature was achieved the tubes were rapidly cooled down (15 °C/min) by opening the furnace lid and switching off the power to the furnace. The resulting carburized sample was ground to a fine powder for characterization.

Synthesis of Bimetallic Oxides. In a typical hydrothermal synthesis of bimetallic oxide represented here by the iron molybdenum system, 0.2 M aqueous solutions of $FeCl_2$ and $(NH_4)_2MoO_4$ were prepared separately by stirring for 15 min. A total of 18 mL of each solution was combined to achieve 80% volume of the reaction chamber and stirred for an additional 15 min before adding to the Teflon cup (45 mL) of an acid digestion vessel from Parr Instrument Company. The acid digestion vessel was incubated at 180 °C for 24 h. The precipitate was recovered by centrifugation and washed three times with deionized water followed by three more times with ethanol. Each washing cycle involved sonication of the sample for 15 min to break up clumps and release soluble impurities prior to centrifugation. The precipitate was dried at 50 °C for 2 h. Finally the product was ground to a fine powder for characterization.

Carbothermic Reduction of Bimetallic Oxide. The as-synthesized bimetallic oxide was combined with decolorizing carbon such that the metal to carbon molar ratio was 1:18 and the mixture ground for 15 min. The rest of the carburization process was analogous to the process described for the reduction of the monometallic oxides above in carbothermic reduction of monometallic oxides.

Carbothermic Reduction in a TGA/DSC Furnace. Both carbothermic reduction processes, with either monometallic or bimetallic oxides, were studied in a TGA/DSC furnace to establish the optimum carburization temperatures and ramping rates. Argon was used as the flow gas at 100 mL/min.

Materials Characterization. X-ray diffraction (XRD) measurements were performed on a Bruker-AXS Smart Apex II CCD diffractometer equipped with an Oxford Cobra Cryosystem utilizing Mo as the X-ray source. Thermogravimetric analysis (TGA) and the corresponding differential scanning calorimetric (DSC) studies were carried out on a SDTQ600 instrument from TA Instruments. Brunauer−Emmett−Teller (BET) method was performed to determine specific surface area on a Micromeritics ASAP2020 instrument using N_2 adsorption data at relative pressure from 0.05 to 0.25. Scanning electron microscopy (SEM) studies were carried out on FEI Quanta FEG 450 field emission scanning electron microscope. The SEM was equipped with a secondary electron detector, a backscattered electron detector, and an Oxford Inca energy dispersive X-ray detector (EDS). All SEM samples were deposited on a carbon tape for analysis, and the acceleration voltage was 20 kV.

■ RESULTS AND DISCUSSION

Bimetallic Carbides from Monometallic Oxides. Bimetallic carbides of W and Mo were synthesized by carbothermic reduction of individual metal oxides with decolorizing carbon. The oxides and carbon were ground together for 20 min to create a homogeneous mixture ensuring that carbothermic reduction can occur throughout the sample uniformly and produce a single phase product. Molar quantities of the oxides and carbon for all systems were based on eq 1.

$$3MoO_3 + Co_3O_4 + 14C \rightarrow Co_3Mo_3C + 13CO \quad (1)$$

The equimolar (TM) carbides of W and Mo occur primarily in two phases, $TM_3(Mo/W)_3C$ and $TM_6(Mo/W)_6C$. Since the precursor mole ratio of carbon to metal depends on which

dx.doi.org/10.1021/cm500076v | Chem. Mater. XXXX, XXX, XXX−XXX

product is formed, the highest carbon to metal ratio was selected as the ideal system to ensure complete reduction of oxides (Table S2, Supporting Information). The carburization reactions were carried out in an oxygen free argon environment, and thus, production of carbon monoxide as a byproduct is more likely than carbon dioxide. This also requires the highest carbon (C) to metal (M) ratio as shown in Table S2, Supporting Information, and was the basis for our precursor calculations.

After grinding, the precursors were annealed at various temperatures in an argon atmosphere to form the bimetallic carbide product. Surprisingly, the low carbon content bimetallic carbides of Fe, Co, and Ni and the corresponding high carbon content bimetallic carbides all form within the temperature window separated by 60 °C (Table S1, Supporting Information). This emphasizes the need for careful control over reaction conditions such as temperature, ramping rate, inert gas flow rate, and cooling rate, in order to form the desired phase pure product.

All the bimetallic carbides discussed here are based on a carbon face centered cubic (fcc) crystal lattice and have been classified eta (η) carbides. The only structural difference between the low carbon content and high carbon content carbides is that the high temperature bimetallic carbides contain twice the number of carbon atoms in the crystal lattice compared to low temperature bimetallic carbides. The increased number of carbon atoms slightly increases the lattice constants of the high carbon content structures. See Table S3 (Supporting Information) for the lattice constants of the bimetallic carbides discussed in this work. This difference in lattice constant can be easily observed by XRD, especially at high angles, allowing reliable phase determination as seen in Figure S1 (Supporting Information).

Unlike in nickel and cobalt systems which yield Ni_6Mo_6C and Co_6Mo_6C, respectively, the corresponding Fe_6Mo_6C phase is not observed in the iron system. The existence of the Fe_6Mo_6C phase has been predicted[29] and claimed without significant evidence.[30,31] It is also of note that the database used during our investigation, ICDD PDF-2 (2012), does not contain any references for the Fe_6Mo_6C phase either. Our investigations reveal that cobalt and iron form the first bimetallic carbide (Co_6Mo_6C and Fe_3Mo_3C, respectively) with molybdenum at 950 °C but nickel requires a slightly higher temperature of 975 °C. This behavior is consistent for the high carbon content phase Ni_3Mo_3C as well. Cobalt and iron phases, Fe_3Mo_3C and Co_3Mo_3C, form at 1010 °C, whereas Ni_3Mo_3C is not observed until 1030 °C. Figure 1 shows the XRD patterns of the low carbon content (a) and high carbon content (b) bimetallic carbide phases of the three Group VIIIA first row TMs with molybdenum.

Contrary to previous attempts to synthesize bimetallic carbides of these three metals of Group VIIIA, our method yields single phase products for each system. To the best of our knowledge, all the methods reported until now are neither universal to all three first row group VIIIA TMs nor devoid of impurities. XRD spectra in Figure 1 show that our method can be employed to synthesize bimetallic carbides of all three TMs with molybdenum reproducibly, with little to no impurities. EDX analysis of the bimetallic carbides, shown in Table S4, Supporting Information, confirm the XRD results in Figure 1, showing that the two TMs involved are in equal atomic percentages throughout the sample. The uniform EDX data also decreases the probability of amorphous monometallic

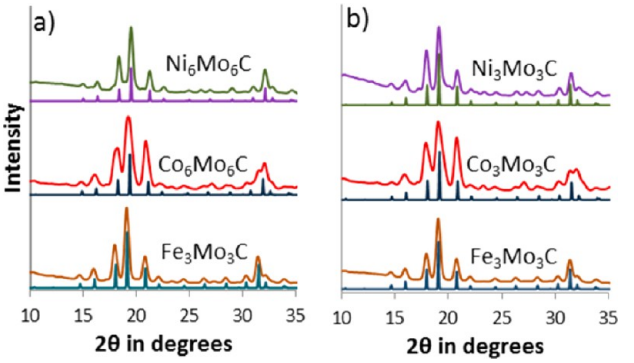

Figure 1. XRD patterns of low (a) and high (b) carbon content bimetallic carbide phases of Ni, Co, and Fe with Mo. The PDF card numbers for reference spectra are Ni_6Mo_6C (04-005-5149), Co_6Mo_6C (04-005-4048), Fe_3Mo_3C (04-005-4038), Ni_3Mo_3C (04-005-4042), and Co_3Mo_3C (04-005-4043).

phases further supporting the determination that the products are single phase crystalline powders of bimetallic carbides.

The synthesis of bimetallic carbides of nickel was particularly challenging. Synthesis attempts based on as-obtained NiO resulted in nickel or nickel carbide impurities in addition to the target bimetallic carbide phase. NiO is the only well-characterized oxide of nickel and is green in color. However, NiO easily degrades to form nonstoichiometric oxides ranging in color from green to dark gray. Another commercially available oxide of nickel is Ni_2O_3, which is a black non-stoichiometric oxide, and it contains a slightly higher percentage of nickel than the formula suggests.[32] Since the as-obtained nickel oxide (NiO) was black in color, we assumed that it was Ni_2O_3 instead of NiO. In order to prepare phase pure bimetallic nickel carbide, a series of experiments with various mole ratios of nickel oxide to molybdenum oxide had to be carried out until neither metallic nickel nor nickel carbide formed. Once the stoichiometric adjustments in the precursor mixture were made from NiO to Ni_2O_3, pure phase Ni_6Mo_6C and Ni_3Mo_3C were obtained on a consistent basis.

Synthetic routes to cobalt molybdenum carbides often produce a mixture of low carbon and high carbon content bimetallic carbide phases. As evident from Figure 1, the peaks on the XRD patterns for our cobalt systems are broader than that of iron and nickel bimetallic carbide systems. Such broadening has been previously assigned merely as impurity with very little discussion.[25,33] This peak broadening could be due to either nanosized domains or the presence of a second bimetallic carbide phase. SEM data, discussed later, shows that the particle size for cobalt systems is comparable to iron and nickel systems, so the broadening observed cannot be assigned solely to smaller particle sizes based on the Sherrer Equation. The XRD peaks of Co_3Mo_3C appear at slightly lower 2θ values than the corresponding peaks of Co_6Mo_6C, due to the increase in lattice constant of the former. Additionally, a careful observation of the two XRD peaks around 31° and 32° 2θ in Figure 1 shows that at lower temperature the XRD peak at 32° is taller (Figure 1a) while at higher temperature the two peaks become of almost similar intensity (Figure 1b). On the basis of lattice constants (Table S3, Supporting Information), it can be concluded that the relative proportion of Co_3Mo_3C with higher lattice constant increases at higher temperature while the lower temperature phase is mostly composed of the smaller lattice constant phase, Co_6Mo_6C.

dx.doi.org/10.1021/cm500076v | Chem. Mater. XXXX, XXX, XXX−XXX

Formation of the corresponding bimetallic carbides of tungsten requires slightly higher temperatures (980 °C) relative to molybdenum systems (950 °C). Unlike the iron molybdenum system, the iron tungsten system occurs in both low carbon content (Fe_6W_6C) and high carbon content (Fe_3W_3C) phases. All three TMs Fe, Ni, and Co investigated here form phase pure low carbon content bimetallic carbides (Figure 2a). The high carbon content phases form at 60 °C higher than the low carbon content phase, analogous to the molybdenum systems. EDX mapping of the bimetallic carbides with tungsten shown in Figure S2 (Supporting Information) show excellent overlap for the two constituent metals.

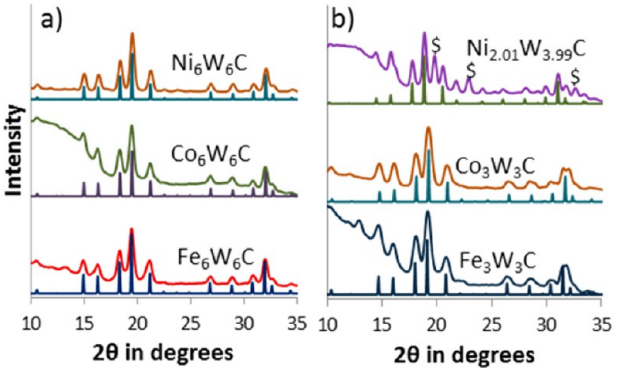

Figure 2. XRD patterns of low (a) and high (b) carbon content bimetallic carbide phases of Ni, Co, and Fe with W. The PDF card numbers for reference spectra are Ni_6W_6C (04-005-4044), Co_6W_6C (04-005-4045), and Fe_6W_6C (04-005-4046), $Ni_{2.01}W_{3.99}C$ (04-005-4041), Co_3W_3C (04-005-4040), and Fe_3W_3C (04-005-4039).

Iron forms phase pure Fe_3W_3C and cobalt Co_3W_3C, but nickel repeatedly formed $Ni_{2.01}W_{3.99}C$ rather than the equimolar Ni_3W_3C. Despite adjusting the stoichiometry of the precursor oxides based on Ni_2O_3 as discussed above, phase pure Ni_3W_3C could not be obtained. However, evidence of the formation of the Ni_3W_3C phase can be seen (Figure S3, Supporting Information). The nickel tungsten carbide system has been studied in detail previously which revealed the existence of Ni_6W_6C and $Ni_{2.01}W_{3.99}C$.[34] In addition to the anomalous stoichiometry of nickel tungsten carbide product, impurities in the form of Ni or NiC also persist, indicated by $ in Figure 2b, even after adjusting the stoichiometry of the precursor oxides to yield $Ni_{2.01}W_{3.99}C$ instead of Ni_3W_3C.

Morphology and Particle Size Distribution. SEM analysis of the bimetallic carbide products reveals submicrometer particles in abundance for most of the tungsten systems, but the molybdenum systems in general have larger particle sizes (Figure 3). This can be attributed to the fact that the precursor molybdenum oxide has an average particle size of almost a micrometer (Figure S4a, Supporting Information) compared to in house prepared tungsten oxide which has particles ranging from 100 to 200 nm (Figure S4b, Supporting Information). Among the group VIIIA metal oxide precursors, Fe_3O_4 had much bigger particle size of almost a micrometer (Figure S4d, Supporting Information) compared to Co_3O_4 and NiO with particle sizes around 50 nm (Figures S4c,e, Supporting Information). Thus, our bimetallic carbides of iron molybdenum systems (Figures 3e,f) have comparatively bigger particle sizes compared to other systems.

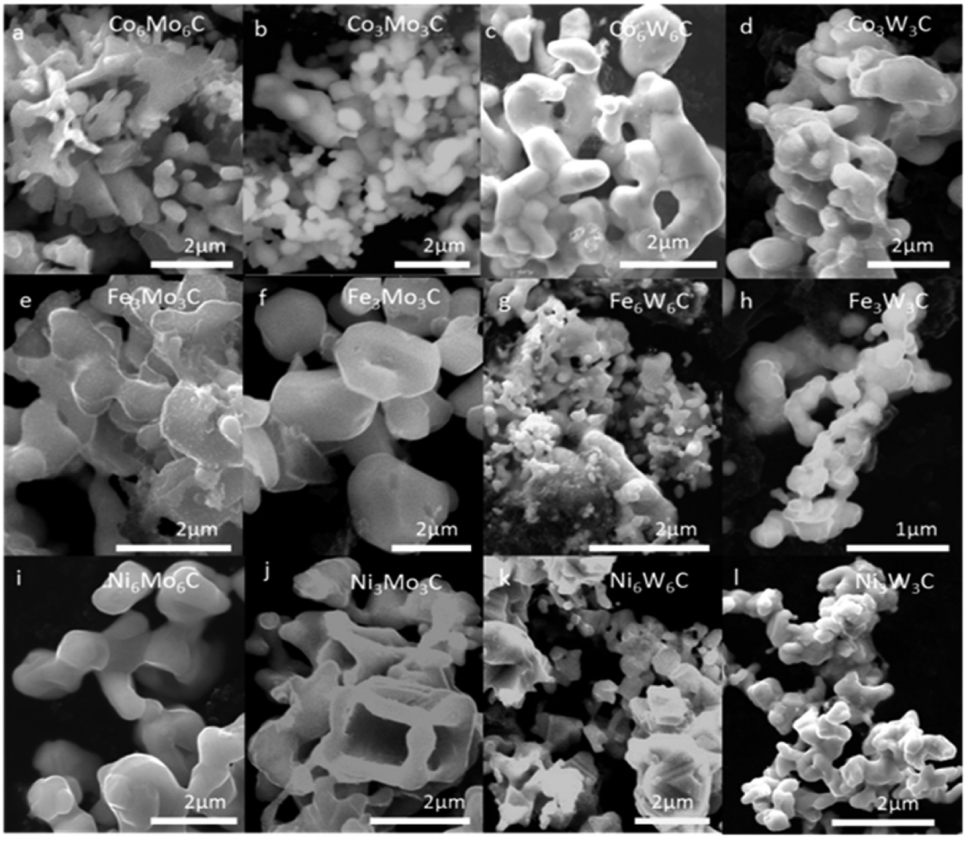

Figure 3. SEM images of various phases of bimetallic carbides of cobalt (a–d), iron (e–h), and nickel (i–l).

dx.doi.org/10.1021/cm500076v | *Chem. Mater.* XXXX, XXX, XXX–XXX

The most prevalent morphology is a network of spherical rods or dumbbells. Although there is variation of size within a sample from submicrometer to few micrometers (Figure 3b), there is a general uniformity in the morphology across this size variation. TM_3Mo_3C systems show very different morphology and size among the three Group VIIIA metals. While Co−Mo−C (Figure 3a,b) mostly has spherical submicrometer particles dispersed with bigger dumbbell shapes, Fe_3Mo_3C (Figure 3e,f) contains biconcave spheres up to a couple of micrometers in diameter. Ni−Mo−C (Figure 3i,j) contains a network of rods of few micrometers in length of submicrometer diameter.

A comparison of the low and high temperature samples of Fe_3Mo_3C shows that the particles size is slightly bigger for the higher temperature 1010 °C sample (Figure 3f) compared to low temperature 950 °C (Figure 3e) sample. Although the crystal structure does not change unlike other systems, there is an observable increase in particle size even within 60 °C.

Influence of Carbon Content on the Dispersion of the Bimetallic Carbides. Catalyst nanoparticles frequently suffer from aggregation due to high surface energies. One common method to prevent nanoparticle agglomeration is to attach the catalyst material on a high surface area support like carbon. To achieve a dispersion of bimetallic carbide particles in a carbon network, an excess of carbon was used in the synthesis instead of the stoichiometric amount based on eq 1. During the course of the investigation, it was observed that an 18 molar excess achieves the optimum dispersion desired. Anything below the 18 molar excess produces big clusters of bimetallic carbides while anything above it severely affects the reproducibility of the desired final product.

BET surface area of cobalt tungsten bimetallic carbides (Table S5, Supporting Information) shows an increase in the specific surface area from the stoichiometric sample 56 m^2/g to 163 m^2/g upon the addition of excess carbon. While we cannot exclude the possibility of excess carbon being present in the stoichiometric samples, very little carbon is observed by SEM (Figure 3). The measured BET surface area of cobalt tungsten carbide samples with higher C:M is much higher due to the presence of a large amount of decolorizing carbon, which has a BET surface area of 585 m^2/g. Even though an accurate carbide surface area cannot be determined, the particle size is greatly decreased in the samples with excess carbon as seen in Figure 4 further proving that the surface area of the bimetallic carbide is indeed increased.

When using 18 molar excess carbon, all the systems investigated here show the tendency to form dispersed arrays of bimetallic carbide particles on a carbon network to various degrees (Figure S5, Supporting Information). SEM analysis showed that the particle size of the bimetallic carbide is in the nanometer range in the dispersed form (Figure 4a) instead of clusters as observed in stoichiometric samples that have dimensions in micrometer range (Figure 4b). In addition, these smaller particles dispersed in carbon undergo less agglomeration because of the carbon network forming a barrier between particles.

Preliminary investigation shows that excess carbon produces a dispersed bimetallic array in all of our synthesized systems; however, the bimetallic particles are not dispersed homogeneously in every sample. Large clusters of bimetallic carbides are present in some samples in addition to the dispersed moieties as in Figure S5e, Supporting Information. Additionally the bimetallic carbides are more difficult to obtain phase pure, unlike when stoichiometric amounts of carbon are used.

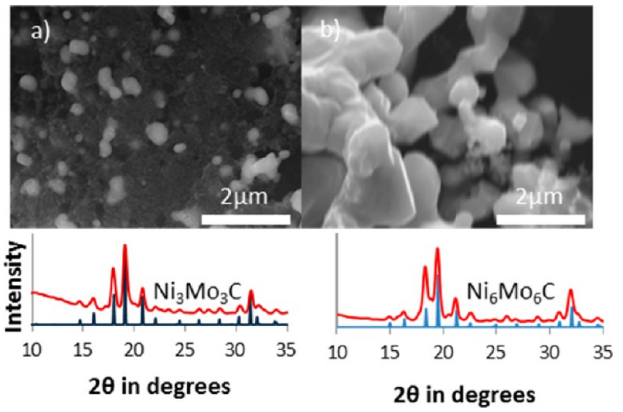

Figure 4. SEM images of bimetallic carbide phases of nickel molybdenum carbide with excess carbon content in starting material (a) and stoichiometric amount of carbon (b). The XRD graphs correspond to the SEM images above them.

It was also observed that a mixture of monometallic carbides were present in addition to the target, single phase bimetallic carbide. One possible explanation for this could be that the excess amount of carbon prevents the precursor oxides from being homogenously distributed at close enough proximity to each other to react and form the bimetallic carbide. Instead the separation by excess carbon results in formation of monometallic carbides. Every sample, however, showed a majority of bimetallic carbide at the temperatures discussed previously.

Synthesis of Bimetallic Carbides from Bimetallic Oxides. One of the ways to circumvent phase separation in the dispersed carbide systems is to first produce nanopowders of corresponding bimetallic oxides and then use carbon to reduce the bimetallic oxides to bimetallic carbides. Zhen et al. in 2008 reported a one-step hydrothermal synthetic route for the preparation of $CoWO_4$ nanorods.[27] Others have reported the synthesis of tungstates and molybdates of other metals.[35,36] The one-step hydrothermal method used for the synthesis of $CoWO_4$ nanorods was adopted to synthesize bimetallic oxides of the six systems discussed in our study, allowing the synthesis of the bimetallic carbide nanopowders.

Iron and cobalt molybdates are phase pure (Figure 5a), but similar purity in nickel molybdate could not be obtained using

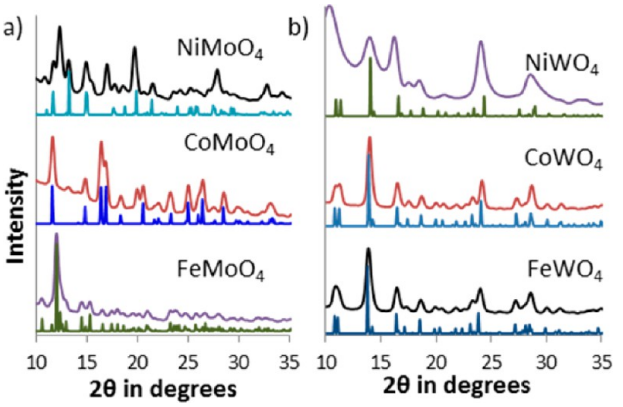

Figure 5. XRD patterns of bimetallic oxide phases, synthesized via solvothermal method, of Ni, Co, and Fe with Mo (a) and W (b). The PDF card numbers for reference spectra are $NiMoO_4$ (00-033-0948), $Co_3Mo_3O_8$ (01-078-7234), $FeMoO_4$ (01-089-267), $NiWO_4$ (00-015-0755), $CoWO_4$ (00-015-0867), and $FeWO_4$ (00-046-1446).

dx.doi.org/10.1021/cm500076v | Chem. Mater. XXXX, XXX, XXX−XXX

our hydrothermal method; however, other methods have been employed previously to synthesize phase pure $NiMoO_4$.[35] Although nickel molybdate was in the final product, MoO_3 and NiO were present as impurities in noticeable quantities (Figure 5a). The ratio of the peaks in the experimental diffraction pattern is slightly different from that of the reference spectra for both nickel and cobalt tungstate (Figure 5b), indicating preferential growth similar to what Zhen et al. reported. In nickel tungstate, the XRD peaks at 17° and 25° are of similar intensity to the peak at 12°. In the reference spectra the XRD peak at 12° is twice the intensity of the ones at 17° and 25°. In cobalt tungstate, the peak at 29° is taller than the peak at 27° in the experimental data, whereas the two peaks are of the same intensity in the reference diffraction pattern (Figure 5b).

Surprisingly, although nickel molybdate is the least phase pure of the three molybdate systems, the corresponding carbide of nickel is the most phase pure of the three systems we synthesized (Figure 6a). Essentially, this reasserts the simplicity

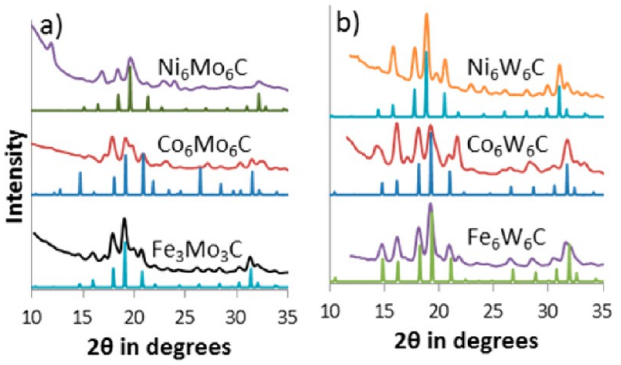

Figure 6. XRD patterns of bimetallic carbide phases, prepared by carburizing the corresponding bimetallic oxides, synthesizes via solvothermal method, of Ni, Co, and Fe with Mo (a) and W (b).

of obtaining phase pure bimetallic carbides from individual oxides as in Figures 1 and 2. Most of the samples obtained via bimetallic oxides contain primarily bimetallic carbide, although the impurities in the form of metals such as iron or nickel, intermetallic alloys such as Ni_4Mo, or monometallic carbides such as Mo_2C are observable by XRD as seen in Figure 6. The broadness of the peaks in the cobalt molybdenum carbide XRD pattern in Figure 6b again shows the tendency to produce a mixture of low carbon content and high carbon content bimetallic carbide phases. Iron molybdenum carbide from bimetallic oxide contains metallic iron impurity indicated by the XRD peak at 19°. Nickel tungsten carbide has some nickel impurity as indicated by the XRD peak at 20°. Iron tungsten carbide is relatively phase pure, but cobalt tungsten carbide synthesized from bimetallic oxide tends to suffer the most among tungsten systems and produces a significant amount of cobalt carbide impurity (Figure 6b).

Our bimetallic oxide route, however, did not result in the dispersion of the bimetallic carbide that was observed with the 18 molar excess of carbon from monometallic oxide synthesis route as seen in SEM images in Figure 7. The EDX maps show complete overlap of the two constituent TMs verifying the bimetallic carbide, but in spite of the bimetallic oxide and carbon mixture having 18 molar carbon excess, there is very little evidence from SEM of nanoparticle dispersion in the carbon network. The temperatures required for formation of

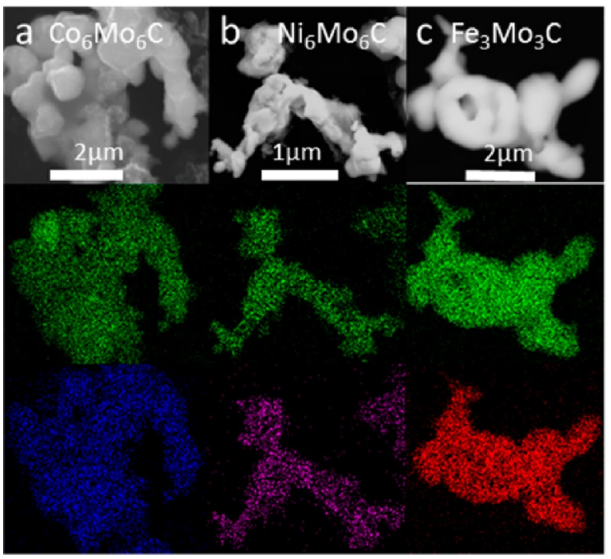

Figure 7. EDX mapping low carbon content bimetallic carbide phases of Co_6Mo_6C (a), Ni_6Mo_6C (b), and Fe_3Mo_3C (c). Green map corresponds to molybdenum while blue, purple, and red correspond to cobalt, nickel, and iron, respectively.

bimetallic carbide via the bimetallic oxide route and monometallic oxide route are the same.

Reduction Pathway from Monometallic Oxide to Bimetallic Carbide. To better understand the reduction pathway for precursor oxides, the formation of cobalt molybdenum carbide was investigated by XRD and TGA/DSC as seen in Figure S6 (Supporting Information) and Figure 8, respectively. Although the reduction process for TPR

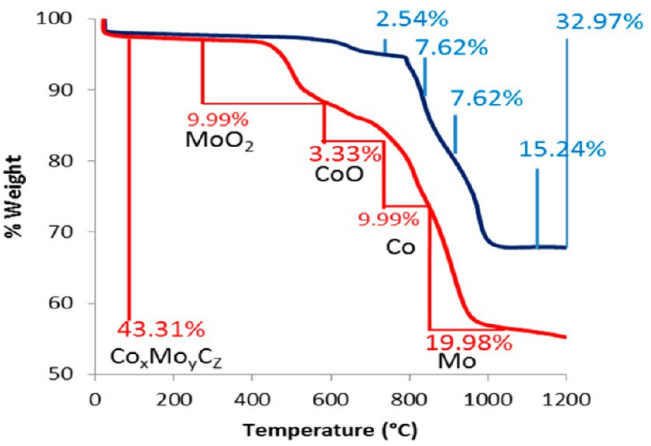

Figure 8. TGA curve for the reduction of a mixture of Co_3O_4 and MoO_3 (lower curve) and Co_3O_4 and WO_3 (upper curve).

reactions of monometallic carbides such as Mo_2C[37,38] and WC[39] have been investigated before, we wanted to gain greater insight into the formation pathway for bimetallic carbides under our reaction conditions.

The TGA curves in Figure 8 below and equations from Table S2 (Supporting Information) show that carbon monoxide is the most likely byproduct, instead of carbon dioxide. The TGA graphs also provide an insight into the reduction pathway.

The total mass losses for both molybdenum and tungsten systems represented in Figure 8 are in excellent agreement with the theoretical mass losses based on eq 1 and the

dx.doi.org/10.1021/cm500076v | Chem. Mater. XXXX, XXX, XXX–XXX

corresponding equation for tungsten system. Co_3O_4 is a mixed valence oxide of cobalt with Co(II) and Co(III) present. From Table S6 (Supporting Information),[40] the electrochemical reduction potentials of each reduction step would suggest that Co(III) would be reduced to Co(II) resulting in a loss of one mole of CO represented by eq 2, which corresponds to 3.33% mass loss.

$$Co_2O_3 + C \rightarrow 2CoO + CO \quad (2)$$

This same event represented by eq 2 should occur analogously in the tungsten system as well. However, the first mass loss event on the molybdenum curve corresponds to a loss of 3 mol of carbon monoxide around 500 °C. It is more likely that the reaction in eq 2 occurs around 625 °C because a mass loss event on the tungsten curve around the same temperature corresponds to the loss of one CO as well. It is more likely that the first thermal event is represented by eq 3. The mole numbers are retained from eq 1 for consistency.

$$3MoO_3 + 3C \rightarrow 3MoO_2 + 3CO \quad (3)$$

Since reduction of Mo(VI) to Mo(IV) takes place before the thermodynamically favored reduction of Co(III) to Co(II) this step must be kinetically favored. Reduction of MoO_3 before Co_2O_3 was further confirmed by XRD (Figure S6, Supporting Information). At 525 °C, the XRD peak at 12° 2θ corresponding to MoO_3 disappears while the peak at 14° (Co_3O_4) persists, confirming our hypothesis that MoO_3 is reduced first.

Similarly, kinetics favors reduction of MoO_2 to Mo before CoO to Co whereas reduction potentials dictate that the appearance of molybdenum metal should precede the appearance of cobalt.

$$3MoO_2 + 6C \rightarrow 3Mo + 6CO \quad (4)$$

$$3CoO + 3C \rightarrow 3Co + 3CO \quad (5)$$

From the TGA graph it is apparent that the three carbon monoxide loss events at approximately 750 °C precedes the six carbon monoxide loss events starting around 850 °C. The XRD peak at 20° which is unique to cobalt metal in the graph (Figure S6, Supporting Information) is present at 775 °C but the XRD peak at 18° which is unique to molybdenum appears only at 825 °C. The Mo reduction temperature is consistent with TPR studies observed during the formation of Mo_2C.[38]

The XRD data also supports the gradual buildup of metallic alloy before the formation of bimetallic carbide based on the XRD peak at 21° corresponding to the Mo−Co alloy. The fact that the XRD peak at 21° (€ symbol) grows in relative intensity compared to the XRD peak at 20° (@ symbol), representative of metallic cobalt, suggests that proportion of the alloy is increasing and metallic cobalt decreasing.

Transition from Low Carbon Content to High Carbon Content Phases. In order to probe the transition from the low carbon content phase to high carbon content phase, we studied the intermediate temperatures by XRD. Not only did the low and high carbon content phases form at temperatures separated by only 60 °C, the transitions proceeded via formation of intermetallic alloy intermediates as shown in Figure 9. Thus it can be concluded that, instead of additional carbon atoms simply inserting into the low carbon content bimetallic carbide crystal lattice, the low carbon content crystal phase completely decomposes and reforms capturing more carbon atoms to form high carbon content crystal structure.

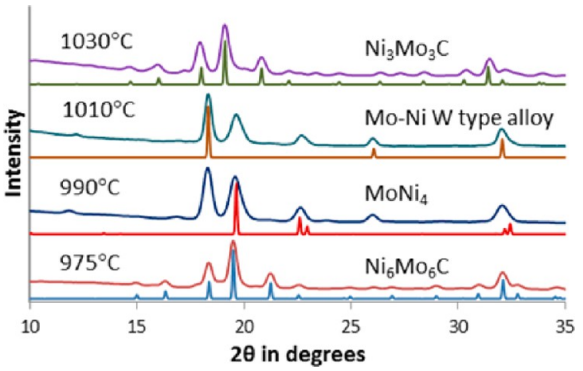

Figure 9. XRD patterns depicting the transition of bimetallic carbide phases of Ni from low carbon content phases to high carbon content phase. The PDF card numbers for reference spectra are Ni_6Mo_6C (01-005-5149), $MoNi_4$ (00-003-1036), Mo−Ni W type alloy (01-071-9769), and Ni_3Mo_3C (04-005-4042).

All of the TM carbides underwent the transformation from low to high via the same mechanism. The low carbon content bimetallic carbide phase separates into intermetallic alloys before the emergence of the high carbon content phase. Bimetallic carbides are known to phase separate into intermetallic alloys and/or monometallic carbides at temperatures beyond their formation temperatures.[41] As an example of the reaction mechanism from low to high carbon content bimetallic carbide, Ni_6Mo_6C forms at 975 °C, but by 990 °C the product phase separates into a mixture of a nickel rich alloy ($MoNi_4$) and molybdenum rich alloy Mo−Ni (W type structure). Mo−Ni W type alloy in the nickel system used in Figure 9 is 98% molybdenum.[42] The stoichiometry in the reference spectra was picked to match the experimental spectra as the reference work listed the value of x in Mo_xNi_{1-x} from 0.985 to 1. These alloys then react with available carbon and reform a metal carbide phase with higher carbon content at 1030 °C.

The temperature dependent fluctuation between bimetallic carbides and intermetallic alloys of various stoichiometries continues beyond the temperatures relevant to our synthesis. In our investigations beyond 1040 °C, we have observed bimetallic carbides of both low and high carbon content type also forming at higher temperatures (Figure S7, Supporting Information). It can be seen that the iron tungsten carbide system forms high carbon content bimetallic phase at 1060 °C and low carbon content phase at 1100 °C. However, these higher temperature phases are relatively less phase pure and contain monometallic carbide impurities such as tungsten carbide. As apparent from Figure S7 (Supporting Information), the high carbon content and low carbon content phases do not form at corresponding lower and higher temperatures unlike the two iron−tungsten phases reported in this investigation at 980 and 1040 °C. The temperatures quoted for our synthesis here represent the lowest temperatures where the low and high carbon content bimetallic carbides can be formed using our method.

■ CONCLUSIONS

We have demonstrated that a common synthesis route can be employed to synthesize bimetallic carbides of Group VIIIA metals with molybdenum and tungsten. Additionally, we have proved that within each system there exist bimetallic carbide phases with high $TM_3(Mo/W)_3C$ and low $TM_6(Mo/W)_6C$

dx.doi.org/10.1021/cm500076v | Chem. Mater. XXXX, XXX, XXX−XXX

carbon contents. The formation of these two phases occurs at temperatures separated by as little as 60 °C. This emphasizes the need to carefully control experimental parameters such as annealing temperature, dwelling time, inert gas flow rate, grinding duration, source of carbon, and ramping rate to improve reproducibility. Utilizing TGA and XRD, an investigation into the reduction route of the precursor oxide revealed that the reduction reaction occurs in a stepwise fashion. We also demonstrate the distribution, size, and morphology of the bimetallic carbide particles can be controlled by varying the carbon content in the precursor mixture which may provide a basis to improve catalyst stability.

■ ASSOCIATED CONTENT

Ⓢ Supporting Information

Additional tables and figures. This material is available free of charge via the Internet at http://pubs.acs.org.

■ AUTHOR INFORMATION

Notes

The authors declare no competing financial interest.

■ ACKNOWLEDGMENTS

We would like to thank the University of Wyoming for start-up funds and the School of Energy Resources for funding.

■ REFERENCES

(1) Zhou, X.; Qiu, Y.; Yu, J.; Yin, J.; Gao, S. *Int. J. Hydrogen Energy* **2011**, *36*, 7398.
(2) Levy, R. B.; Boudart, M. *Science* **1973**, *181*, 547.
(3) Lee, J. *J. Catal.* **1987**, *106*, 125.
(4) Eckstrom, H. C.; Adcock, W. A. *J. Am. Chem. Soc.* **1950**, *72*, 1042.
(5) He, Z.; Maurice, J.-L.; Gohier, A.; Lee, C. S.; Pribat, D.; Cojocaru, C. S. *Chem. Mater.* **2011**, *23*, 5379.
(6) Weller, S.; Hofer, L. J. E.; Anderson, R. B. *J. Am. Chem. Soc.* **1948**, *70*, 799.
(7) Alexander, A. M.; Hargreaves, J. S. *Chem. Soc. Rev.* **2010**, *39*, 4388.
(8) *The Chemistry of Transition Metal Carbides and Nitrides*, 1st ed.; Oyama, S. T., Ed.; Blackie Academic & Professional: Glasgow, 1996.
(9) Lee, J. S.; Locatelli, S.; Oyama, S. T.; Boudart, M. *J. Catal.* **1990**, *125*, 157.
(10) Barbir, F. *PEM Fuel Cells*, 2nd ed.; Academic Press: London, 2013.
(11) Zhang, J.; Tang, S.; Liao, L.; Yu, W. *Chin. J. Catal.* **2013**, *34*, 1051.
(12) Volpe, L.; Boudart, M. *J. Solid State Chem.* **1985**, *59*, 332.
(13) Da Costa, P.; Lemberton, J.-L.; Potvin, C.; Manoli, J.-M.; Perot, G.; Breysse, M.; Djega-Mariadassou, G. *Catal. Today* **2001**, *65*, 195.
(14) Scholl, H.; Hofman, B.; Rauscher, A. *Electrochim. Acta* **1992**, *37*, 447.
(15) Mohan, K.; Strutt, P. R. *Nanostruct. Mater.* **1996**, *7*, 547.
(16) Xiao, T. *J. Catal.* **2002**, *209*, 318.
(17) Puello-Polo, E.; Brito, J. L. *J. Mol. Catal. A: Chem.* **2008**, *281*, 85.
(18) Liu, Y.; Kelly, T. G.; Chen, J. G. G.; Mustain, W. E. *ACS Catal.* **2013**, *3*, 1184.
(19) Ma, X.; Meng, H.; Cai, M.; Shen, P. K. *J. Am. Chem. Soc.* **2012**, *134*, 1954.
(20) Fraker, A. C.; Stadelman, H. *Trans. Metall. Soc. AIME* **1969**, *245*, 847.
(21) Volpe, L.; Boudart, M. *J. Solid State Chem.* **1985**, *59*, 348.
(22) Alconchel, S.; Sapina, F.; Martinez, E. *Dalton Trans.* **2004**, 2463.
(23) Michalski, A.; Siemiaszko, D. *Int. J. Refract. Met. Hard Mater.* **2007**, *25*, 153.
(24) Korlann, S.; Diaz, B.; Bussell, M. E. *Chem. Mater.* **2002**, *14*, 4049.
(25) Wang, X.-H.; Zhang, M.-H.; Li, W.; Tao, K.-Y. *Catal. Today* **2008**, *131*, 111.
(26) Shao, Y.; Yin, G.; Gao, Y. *J. Power Sources* **2007**, *171*, 558.
(27) Zhen, L.; Wang, W.-S.; Xu, C.-Y.; Shao, W.-Z.; Qin, L.-C. *Mater. Lett.* **2008**, *62*, 1740.
(28) Moura, A. P. d. *Adv. Chem. Eng. Sci.* **2012**, *02*, 465.
(29) Goldschmidt, H. J. *Interstitial Alloys*; Butterworths: London, 1967.
(30) Lad'yanov, V. I.; Sterkhova, I. V.; Kamaeva, L. V.; Chueva, T. R.; Molokanov, V. V. *J. Non-Cryst. Solids* **2010**, *356*, 65.
(31) Mccandlish, L. E.; Kugler, E. L.; Jacobson, A. J.; Chianelli, R. R. Google Patents, 1994.
(32) Greenwood, N. N. *Chemistry of the elements*, 2nd ed.; Butterworth-Heinemann: 1984.
(33) Xiao, T. *J. Catal.* **2001**, *202*, 100.
(34) Cury, R.; Joubert, J. M.; Tusseau-Nenez, S.; Leroy, E.; Allavena-Valette, A. *Intermetallics* **2009**, *17*, 174.
(35) Chen, M.; Wu, J.-L.; Liu, Y.-M.; Cao, Y.; Guo, L.; He, H.-Y.; Fan, K.-N. *J. Solid State Chem.* **2011**, *184*, 3357.
(36) Shim, H. W.; Cho, I. S.; Hong, K. S.; Cho, W. I.; Kim, D. W. *Nanotechnology* **2010**, *21*, 465602.
(37) Oyama, S. T. *Catal. Today* **1992**, *15*, 179.
(38) Guil-López, R.; Nieto, E.; Botas, J. A.; Fierro, J. L. G. *J. Solid State Chem.* **2012**, *190*, 285.
(39) Löfberg, A.; Frennet, A.; Leclercq, G.; Leclercq, L.; Giraudony, J. M. *J. Catal.* **2000**, *189*, 170.
(40) *Standard Potentials in Aqueous Solution*; Bard, A. J., Parsons, R., Jordan, J., Eds.; Marcel Dekker, Inc.: New York, 1985.
(41) Dubrovinskaia, N. A.; Dubrovinsky, L. S.; Saxena, S. K.; Selleby, M.; Sundman, B. *Journal of Alloys and Compunds* **1999**, *285*, 242.
(42) Harker, D. *J. Chem. Phys.* **1944**, *12*, 315.